Imaging Test Setup of HXMT*

DONG Yong-Wei[1,2;1)] WU Bo-Bing[1] LI Yan-Guo[1] ZHANG Yong-Jie[1] HE Hui-Lin[1] WU Mei[1]

1 (Key Laboratory of Particle Astrophysics, Institute of High Energy Physics, CAS, Beijing 100049, China)
2 (The Graduate School of the Chinese Academy of Sciences, Beijing 100049, China)

Abstract The imaging test setup for the Hard X-ray Modulation Telescope (HXMT) mission was built to give verification of detector performance and the imaging properties of HXMT. It consists of 18 slat-collimated NaI(Tl)/CsI(Na) phoswich detectors with a total collective area of 5000cm^2. Several experiments were implemented with radioactive sources 15m away from the detector plane. We obtained a point-source location accuracy of 2' and an angular resolution of <5' using direct demodulation method.

Key words HXMT, direct demodulation, imaging test setup

1 Introduction

The space observation of hard X–rays with photon energies from 10keV to several hundred keV is an important approach to study high energy process in celestial objects. But all-sky survey of this energy range has been very limited so far.

Based on the Direct Demodulation (DD) method[1] and collimated phoswich instruments, the Hard X-ray Modulation Telescope (HXMT) mission has been proposed. With both high sensitivity and high spatial resolution, HXMT is capable of making wide-field hard X-ray imaging, including hard X-ray all-sky survey，deep surveys of selected sky regions with angular resolution of 5' and location accuracy of 1', or pointed observations for spectroscopy and timing studies of sources. The expected sensitivity of HXMT at 100keV is $3\times10^{-7}\mathrm{cm}^{-2}\cdot\mathrm{s}^{-1}\cdot\mathrm{keV}^{-1}$.

The HXMT imaging test setup has been built. We aim to do scanning experiments with this setup and to make a ground checkout of HXMT performance using DD method.

2 The HXMT imaging test setup

This setup runs with four parts included: the payload, the servomechanism, data transferring sub-system and data processing sub-system, and they are connected to the Local Area Network.

In our prototype, the payload consists of 18 detector modules (Fig. 1). Each module is made up of one cylindrical NaI(Tl)/CsI(Na) scintillation detector, one collimator, one PMT and their shield. The collective area of a detector is 283.5cm^2. The NaI as

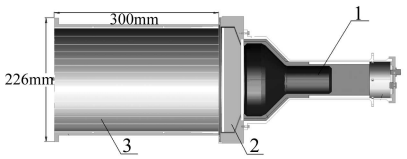

Fig. 1. An architecture of detector module.
1: PMT; 2: Phoswich; 3: collimator.

the main detector has a thickness of 3.5mm, while the active shielding CsI(Na) is 40mm thick. These detectors operate in the energy range of 20—250keV and in photon counting mode. The scintillation events can be classified by the place where photons deposit energy. Those only deposit energy in the NaI crystal are accepted, others are rejected. The pulse shape discrimination is capable of identifying these events according to their different decay constants. A 2mm thick Be slice or a Al slice clings to the phoswich as

Received 12 September 2005, Revised 29 December 2005
*Supported by Major State Basic Research Development Program (G2000077600) and NSFC (10327301, 10473011)
1) E-mail: dongyw@mail.ihep.ac.cn

the incident window. A 5-inch PMT is used to collect the fluorescence of phoswich.

A wide Field of View (FOV) could increase the incident events when scanning. While too wide a FOV in the hard X-ray range reduces the angular resolution and the location accuracy of detectors. The background caused by aperture incident photons could dominate over the other background components with a much large FOV. Rectangular units are used in each collimator. The collimator limits the detector field of view to $5.7^\circ \times 1.1^\circ$ (FWHM). However the directions of long axes of FOVs vary with a step-size of 10° which is proved by simulation to improve imaging of numerous sources. So eighteen collimators define the FOV to be $5.7^\circ \times 5.7^\circ$. The dimension of rectangle units in collimators is 32mm × 6mm. The thin slat along the 1.1° direction is Ta with a thickness of 0.15mm and the other slat made of Pb-Sb alloy is 3mm thick.

Only active shielding is used because of a low level of background particles. While in HXMT mission we must add on passive shielding for detectors. PMTs are generally very susceptible to magnetic fields, especially for head-on types. So we enveloped the PMTs with permalloy which can sufficiently eliminate the effect of the terrestrial magnetism.

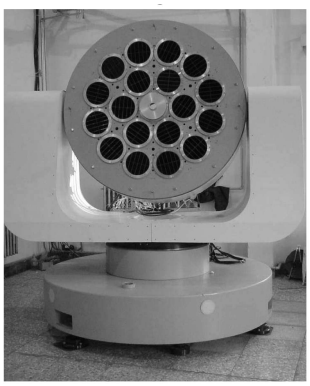

Fig. 2. Photograph of the detector plane mounted on a platform.

The attitude of detectors is controlled by a double-axes rotational platform (Fig. 2) which can move in both azimuth and elevation direction. So satellite motion in the orbit and precession of orbit plane are imitated. A location accuracy of 1' can be approached by this platform. We use radioactive ^{241}Am to act as the X-ray source in outer space. The radioactive sources are placed on a xy-plane 15m away from our payload platform (Fig. 2). Since there exists X-ray scattering and absorbing effect in the air, not a too long distance is selected.

3 Data deconvolution

DD method is used in our imaging. The DD technique performs a deconvolution from scanning data by iteratively solving modulation equation $Pf = d$ under proper physical constraints. P is the point spread function, f is the object intensity and d gives the observational data. The formula of DD algorithm by using the Richardson-Lucy (RL) iterations[2] is

$$f^{(r+1)}(k) = f^{(r)}(k) \times \sum_{i=1}^{M} \left(p(i;k) \cdot \frac{d(i)}{d^{(r)}(i)} \right), \quad k = 1,2,\cdots N,$$

$$d^{(r)}(i) = \sum_{k=1}^{N} p(i;k) f^{(r)}(k), \quad i = 1,2,\cdots M, \qquad (1)$$

with the constraint condition

$$f(k) \geqslant b(k),$$

where i $(1 \sim M)$ is the observing point of detectors, k $(1 \sim N)$ is the element in image space, r is the iteration step, and the lower intensity limit $b(k)$ is the background intensity. Here the RL method is chosen as the algorithm which is more feasible to do point-source imaging.

The equation used in deconvolution is written as

$$f^{(r+1)}(k,l) = f^{(r)}(k,l) \times \sum_{c,i,j} \left(\frac{p(c,i,j;k,l)}{\sum_{cc,ii,jj} p(cc,ii,jj;k,l)} \cdot \frac{d(c,i,j)}{d^{(r)}(c,i,j)} \right), \qquad (2)$$

$$d^{(r)}(c,i,j) = \sum_{kk,ll} (p(c,i,j;kk,ll) \cdot f^{(r)}(kk,ll)) + b(c,i,j),$$

where c represents the number of collimator, (i,j) is the observing point of detectors, (k,l) indicates the element in image space. The difference between Eq. (1) and Eq. (2) is how to add in the physical constraints. In Eq. (1), the constraint is defined in image space; While in Eq. (2), the constraint is described in observation space. They are equivalent only when the image space is large enough to cover the viewing field at each scanning point. The background distribution

in observation space is measured to be approximatively uniform by our experiment.

4 Measurement and calibration

There are eighteen detectors mounted together on the setup. Each detector has its particular parameters. We obtained their values for better image deconvolution. Energy responses were first calibrated. The calibration was done by adjusting high voltage of PMT with the detector exposed to a radioactive source. As a result, high voltages of 18 detectors vary from 900V to 1200V to get a uniform energy response peak at channel 50. The spectrum has 256 channels.

Different background levels represent different physical constraints used in DD iteration; Background of one detector doesn't vary with orientation.

Table 1. Background count rate(20—250keV).

detector No.	1	2	3	4	5	6
count rate(cps)	9.37	8.92	8.36	7.28	9.34	9.81
detector No.	7	8	9	10	11	12
count rate(cps)	10.36	11.80	10.97	10.04	7.02	8.59
detector No.	13	14	15	16	17	18
count rate(cps)	8.41	7.68	8.76	10.31	11.50	11.46

The responses of counts to sources are not uniform. We fixed one 1mCi source on the source plane, and made a one-dimension survey of this source using every detector. The track's direction is parallel to 1.1° direction of the collimator. The center point of track is just across the normal of the corresponding detector plane.

A count rate of 40counts/s/μCi when incidence angle equals 0° has been obtained with MC simulation using GEANT3 software. In unit of this expected count rate, Fig. 3 shows the experimental count rate from 6 out of 18 tested detectors as a function of incidence angle. Values at angle = 0° give the different responding factors which are added into Point Spread Function (PSF) of detectors. All peak values are lower than the result of simulation because of defective crystals.

Then several scanning experiments were carried out. We designed the track map to get enough exposure at different angles for every detector. With the platform tracking like a snake (Fig. 4), we got a count curve shown in Fig. 5.

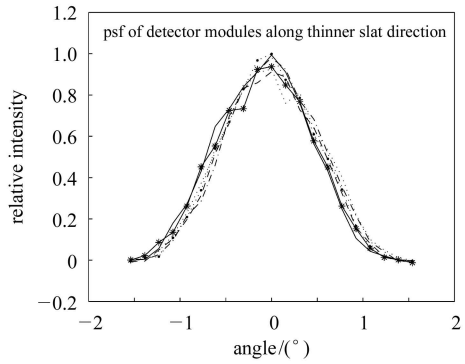

Fig. 3. Comparision of counts responses. 6 out of 18 count curves are shown.

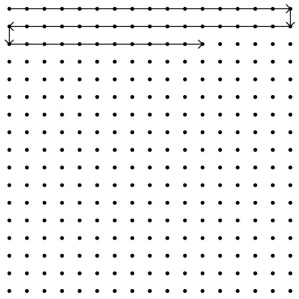

Fig. 4. A sketch of scanning observation. At each point the platform stays still for several seconds.

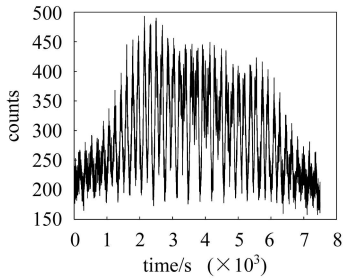

Fig. 5. A count curve of detectors. Each peak corresponds to a horizontal line in Fig. 4.

5 Results

5.1 Sensitivity of the test setup

The continuum sensitivity of detectors can be obtained by the following formula[3]:

$$F_{\min}=\frac{n_\sigma}{\varepsilon}\cdot\sqrt{\frac{4B}{AT\Delta E}}\mathrm{cm}^{-2}\cdot\mathrm{s}^{-1}\cdot\mathrm{keV}^{-1}, \qquad (3)$$

where $n_\sigma = 3$, $A = 5100\mathrm{cm}^2$, $T = 10^5\mathrm{s}$, $\Delta E = E$, ε is the detection efficiency, B is the background of

all detectors. Background spectrum of one detector is shown in Fig. 6. We set the threshold energy to 15keV. The spectrum has a power-law shape caused by cosmic-ray aperture background. Two peaks in the graph represent K-shell emission lines of Pb at the energy 75.0keV and Ta at 57.5keV. The other material of collimators is Sb and its emission line at 26.1keV is hard to recognize because of low proportion in the alloy. We could get a weaker fluorescence peak adding Sn at the bottom of collimators which was supported by Geant4 simulation. The sensitivity of the test setup is worse than HXMT simulation because of higher background level. Some incident windows made of Al increase the background as well. Table 2 shows the sensitivity of our setup.

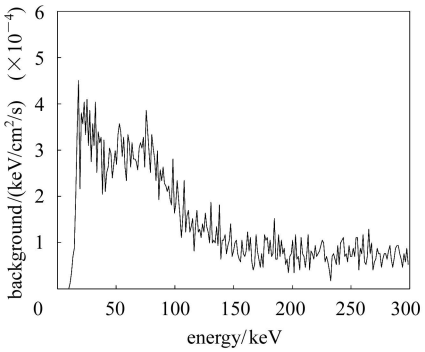

Fig. 6. Background spectrum. Data of one detector with Be window is used.

Table 2. Continuum sensitivity of HXMT imaging setup.

energy/keV	20	30	40	50	60	70
sensitivity/($\times10^{-7}$) ($\mathrm{cm^{-2}\cdot s^{-1}\cdot keV^{-1}}$)	15.6	11.8	8.36	6.83	6.74	6.22
energy/keV	80	90	100	150	200	250
sensitivity/($\times10^{-7}$) ($\mathrm{cm^{-2}\cdot s^{-1}\cdot keV^{-1}}$)	6.08	5.16	4.97	5.97	7.41	8.55

The Crab spectrum(10keV—10MeV) is given by[4]:

$$\frac{\mathrm{d}N}{\mathrm{d}E}=23.8E^{-2.3}\mathrm{cm^{-2}\cdot s^{-1}\cdot keV^{-1}}. \quad (4)$$

After an integral over the energy band 20—250keV, the Crab count rate in out setup would be 1478count/s by taking into account the detecting efficiency of the setup; Table 1 gives an overall background of 170count/s. So we get a minimum detectable source intensity of 0.8count/s for 3σ significance and 2400s observation time, which also means a 0.54mCrab source or a 0.2μCi radioactive source 15m away from our setup considering the efficiency. Simulated data are generated using the photon tracing method, and we've only reconstructed a lowest detectable source with the intensity of 10μCi. The reasons for the higher value are: the finite distance between source and detectors decreases the detection ability; the S/N value is lower when the setup is scanning than when it is aiming at the source.

5.2 Single source experiment

We performed an experiment with a 100μCi ^{241}Am source. The source was at (0, −0.382°) in the instrument reference frame. A region of 11°×11° was scanned with a grid distance of 0.22° and a total observation time of 2400s.

Because the DD process is non-linear, the direct error estimation is difficult to make. We use bootstrap method[5—7] to overcome this problem. Assume that we have primary scanning data with P events. First we make sampling with replacement for P times and regroup P samplings into a new data map; Then do $N=1000$ DD iteration steps on each picture; Repeat the above steps for $M=200$ times and we get M restored images; From these images we get the statistical parameters, such as position accuracy and source intensity. One image is shown in Fig. 7.

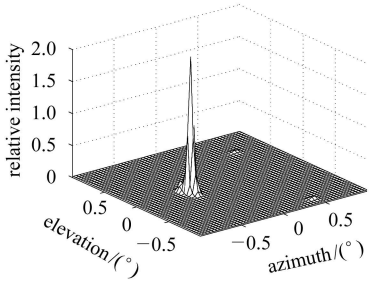

Fig. 7. The reconstructed image of single source after 1000 iteration steps. The distance between imaging points is 0.038°. $n_\sigma=27$.

The source we demodulated from M pictures is at (0.009°, −0.412°). 68% of the 200 bootstrap samples locate within ±0.036° of the mean (Fig. 8), so half of this range, 2', is a good estimate of the point-source position accuracy. The value of angular resolution (FWHM) has been tested to be much smaller than that of the intrinsic angular resolution 1.1°. Results

indicate that it is better than 5' with a grid distance of 0.038° in imaging. From Fig. 9 we are 68% confident that the intensity of source is between 100.1μCi and 106.5μCi. Meanwhile, the values of parameters depend on the iteration steps, the total counts of observation, the distribution of the source, the background level and so on.

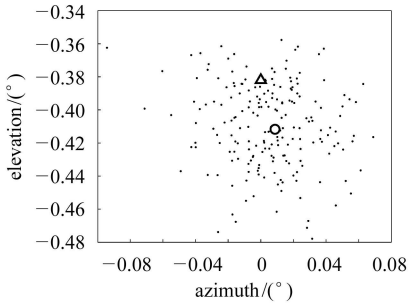

Fig. 8. Distribution of the source centroid from M images. Triangle represents the real position. Circle represents the result of primary scanning data.

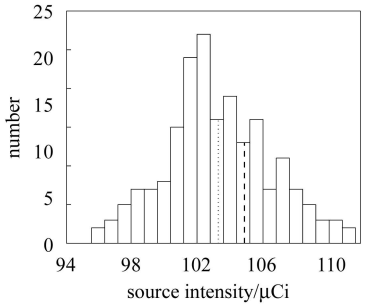

Fig. 9. Frequency distribution of source flux got from $M = 200$ images. The dotted line marks the mean of the bootstrap means. The dashed line gives the result from primary scanning data.

5.3 Multisource experiment

The intensities of ^{241}Am sources used in experiments are 2mCi, 1mCi, 1mCi and 0.1mCi. Fig. 10 and Fig. 11 give the restoration results. By adding up the counts more than 10% of the peak count of a source in the restored image, we calculated out the intensities of four sources to be 2.19mCi, 1.06mCi 0.99mCi and 0.102mCi. Bigger error of stronger sources than weaker sources might come from different dispersion of sources. The distance between 2mCi source and 1mCi one is 0.64° and that between 1mCi and 0.1mCi is 0.78°.

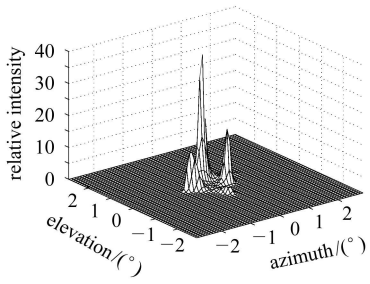

Fig. 10. The experimental result of four sources.

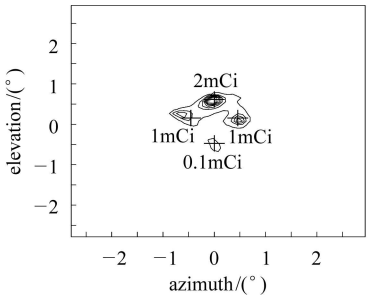

Fig. 11. The experimental result of four sources: Cross represents the real position.

6 Summary

It's the first time in the world to carry out ground-based imaging of radioactive sources using collimators. There are differences between imaging with detectors being at an infinite distance and at a finite distance from sources. The imaging ability surely will be decreased. The calibration of location still has some problems which make error difficult to give out. We demonstrated that this setup has good capability to locate point-source and to determine the intensities of multiple point sources. The location accuracy of 2' and angular resolution of 5' obtained from DD method give a strong support to HXMT mission.

References

1 LI T P, WU M. AP&SS, 1993, **206**: 91
2 Lucy L B. AJ, 1974, **79**: 745
3 WANG J Z. PhD Thesis at IHEP, 1994. 129
4 Zombeck M V. Handbook of Space Astronomy and Astrophysics. UK Cambridge University Press, 1990. 215
5 Efron B. Ann. Statistics, 1979, **7**: 1
6 Diaconis P, Efron B. Scientific American, 1983, Sept., 96
7 LU F J et al. Acta Astron. Sinica, 1997, **38**(1): 56—66 (in Chinese)
(卢方军等. 天文学报, 1997, **38**(1): 56—66)

HXMT卫星地面样机成像实验*

董永伟[1,2;1)]　吴伯冰[1]　李延国[1]　张永杰[1]　何会林[1]　吴枚[1]

1 (中国科学院高能物理研究所　北京　100049)
2 (中国科学院研究生院　北京　100049)

摘要　硬X射线调制望远镜(HXMT)致力于实现硬X射线能段的高灵敏度巡天. HXMT地面样机已在中国科学院高能物理研究所粒子天体物理重点实验室建成. 它包括18个栅条准直的NaI(Tl)/CsI(Na)复合晶体探测器, 总有效探测面积为5000cm^2. 探测器工作在20—250keV, 视场范围5.7°×5.7°通过近距离放射源成像实验和直接解调成像方法的使用, 地面样机能够达到2'点源定位精度和5'角分辨率(FWHM).

关键词　HXMT　直接解调成像方法　地面样机成像

2005 – 09 – 12 收稿,　2005 – 12 – 29 收修改稿
*国家重点基础研究发展规划项目(G2000077600)和国家自然科学基金(10327301, 10473011)资助

1) E-mail: dongyw@mail.ihep.ac.cn